analytical chemistry

pubs.acs.org/ac Article

Efficient Curing Sacrificial Agent-Induced Dual-Heterojunction Photoelectrochemical System for Highly Sensitive Immunoassay

Min Chen, Fangjing Mo, Hui Meng, Cun Wang, Jiang Guo, and Yingzi Fu*

Cite This: *Anal. Chem.* 2021, 93, 2464−2470 Read Online

ACCESS | Metrics & More | Article Recommendations | Supporting Information

ABSTRACT: A photoelectrochemical (PEC) biosensor is a very efficient and sensitive detection technology for the quick and effective conversion of light to electrical signals. However, the sensitivity and stability of the sensors are still unsatisfactory based on single-phase semiconductors or in the absence of sacrificial agents in the test solution. Herein, we present an efficient curing sacrificial agent-induced dual-heterojunction PEC system, which can detect the prostate-specific antigen (PSA) with high sensitivity. This PEC immune system was initially fabricated using single-walled carbon nanohorns (SWCNHs), p-type MoS_2, and n-type Ag_2S successively through a Schottky junction and p−n heterojunction on a glassy carbon electrode with electrodeposited gold nanoparticles. Then, the capture antibody (Ab1) was modified and the nonspecific binding sites were sealed off. Meanwhile, the ferrocene (Fc) solidified with hollow nanospheres of zinc ferrite ($ZnFe_2O_4$) served as a curing electronic sacrificial agent (Fc-$ZnFe_2O_4$). Next, the detection antibody labeled with Fc-$ZnFe_2O_4$ (Ab2-Fc-$ZnFe_2O_4$) was used as a bio-nanoprobe and captured by PSA and Ab1 via sandwich immunorecognition. Under white light, PEC signal amplification could be driven by the curing electronic sacrificial agent-induced dual-heterojunction to achieve the highly sensitive detection of the target. This proposed system exhibited excellent photocurrent performance within the working range from 1 fg·mL^{-1} to 100 ng·mL^{-1} at a low detection limit of 0.44 fg·mL^{-1} (S/N = 3). The proposed strategy features high sensitivity, selectivity, and stability that provides a new opportunity for the development of biosensors in the PEC field.

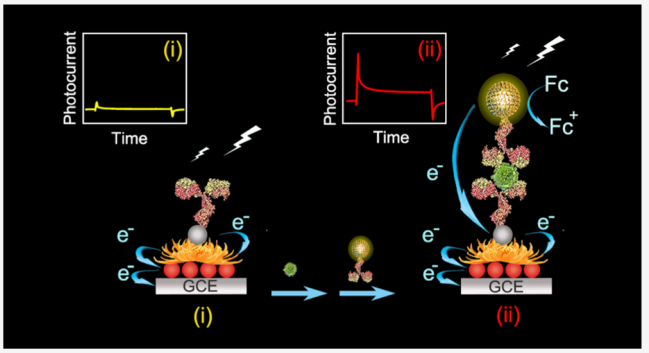

Photoelectrochemical (PEC) biosensors that relied on semiconductors feature high sensitivity, good selectivity, relatively simple equipment, and easy miniaturization, becoming a prospective analysis method.[1] Nevertheless, most single-phase semiconductors are limited in practical application due to the poor conductivity and low efficiency of hole and photoelectron separation.[2] PEC signals can be amplified by improving the photoelectric conversion efficiency of semiconductor materials through doping, changing the morphology of semiconductors, forming heterojunctions, adding sacrificial agents in the test solution, or modifying organic sensitizers.[3,4] Moreover, the semiconductors with a heterojunction structure also possess a high efficiency photoelectric conversion effect attributed to the effective separation between photoelectrons and holes in the built-in electric field, which is a very advisable choice to construct a biological analysis PEC system.[5−7] Numerous carbon materials, because of their good conductivity, biocompatibility, low price, easy functionalization, and environmental friendliness, are widely applied in biological imaging, nanomedicine, batteries, biosensors, etc.[8−10] Novel optoelectronic materials, which combine carbon materials with semiconductors by a Schottky junction structure, have attracted great attention in the field of optoelectronics.[11,12] Under the excitation of light, the photogenerated electrons of semiconductors are separated from the holes, migrated away, and captured by the Schottky barrier.[13,14] The results show that these semiconductors with the Schottky junction structure are conducive to the photocatalytic reaction.[15] As one of the carbon nanomaterials, single-walled carbon nanohorns (SWCNHs) have good potential in constructing Schottky junction optoelectronic materials with semiconductors due to their high purity and large specific surface area.[16,17]

Owing to the large built-in electric field of p−n heterostructure materials, the photoelectric conversion efficiency can be greatly improved, which brings about a widening light absorption range and reducing the requirement for raw materials.[18] As the outstanding optoelectronic materials, p-type MoS_2 and n-type Ag_2S semiconductors with good biocompatibility are the appropriate candidates to fabricate p−n heterostructure nanocomposites in the biological analysis

Received: October 23, 2020
Accepted: December 24, 2020
Published: January 5, 2021

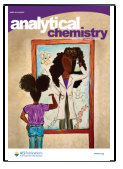

https://dx.doi.org/10.1021/acs.analchem.0c04485
Anal. Chem. 2021, 93, 2464−2470

PEC system.[19,20] In addition, sacrificial agents are frequently added in the test solution of a traditional PEC system, which can consume electrons or holes on the surface of semiconductors, effectively separate electrons from holes, and improve the photoelectric conversion efficiency.[21,22] Meanwhile, some adverse effects are invariably introduced. For instance, unstable signals are caused by the concentration change of sacrificial agents, which come from the PEC reaction or oxidation−reduction; the large background signals are caused by the PEC reaction without permission, and the pollution of the biochemical interface are caused by the interaction with biomolecules on the sensor's surface.[23] To overcome these adverse effects, some sacrificial agents with protective groups or some sacrificial agents encapsulated in liposomes which labeling with biomolecules have been used for target detection. These sacrificial agents can be released to participate in the PEC reaction by enzyme hydrolysis or dissolution of liposomes in situ.[24−27] Our group has developed a curing sacrificial agent combined with the reductive sulfite and nanogold for immune detection.[28] Although these methods have been performed free of sacrificial agents in the test solution, they still face some challenges, such as complex actual operation, an increased cost, and unfriendly biological detection interfaces. Ferrocene (Fc) is used as an electron sacrificial agent due to its inherent electrochemical properties and strong conductivity for the electron-rich system.[29,30] But until now, Fc-functionalized nano-semiconductor zinc ferrite (Fc-$ZnFe_2O_4$) serving as a curing electronic sacrificial agent to meet the PEC immunoassay requirements has rarely been reported.

Here, we report a novel sandwich immunorecognition PEC system based on the dual-heterojunction induced by a curing sacrificial agent for the sensitive detection of the prostate-specific antigen (PSA) (Scheme 1A). When the PEC immunosensor is incubated with the PSA and Fc-$ZnFe_2O_4$ labeled prostate detection antibody (Fc-$ZnFe_2O_4$-Ab2) successively, an amplified signal can be received (Scheme 1B,D).

Scheme 1. (A) Preparation Procedure of a Dual-Heterojunction Immunosensor. (B) Signal generated by Electron Transfer after the Sandwich Immunorecognition for PSA Detection under White Light. (C) High-Resolution Transmission Electron Microscopy (HRTEM) Image of the Partial Fc-$ZnFe_2O_4$ Structure. (D) Photocurrent of the Immunosensor (i) before and (ii) after Incubation with the Target and Ab2-Fc-$ZnFe_2O_4$

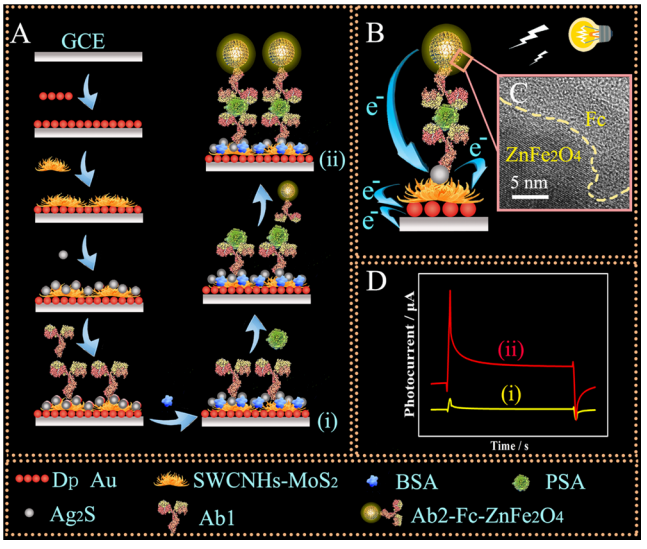

EXPERIMENTAL SECTION

Chemicals and Apparatus. Single-walled carbon nanohorns (SWCNHs, 97.0%) were bought from the Chemical Reagent Co. (Chongqing, China). The prostate-specific antigen (PSA) and antibody (Ab) were purchased from J&K Chemical Co. (Beijing, China). All reagents purchased from regular commercial suppliers were used in this study without further purification. Details about the other products are given in the Supporting Information (SI). Double distilled water (18.2 MΩ·cm) was used throughout this experiment.

PEC detection was carried out on a CHI 440A electrochemical workstation (Shanghai Chenhua Instruments Co., China), which configured an external LED lamp with the output power of about 14 $mW{\cdot}cm^{-2}$ in 4 mL of 0.1 M phosphate buffer saline (PBS, pH 7.4). Details of other apparatus are provided in the SI. All measurements were carried out at the room temperature of 25 ± 1 °C.

Solvothermal Synthesis of SWCNHs-MoS_2. The SWCNHs-MoS_2 composite was synthesized according to a previous report with some modifications.[31] A quantity of 8.5 mg of SWCNHs was dispersed into 20 mL of 0.2% sodium dodecyl benzene sulfonate aqueous solution with ultrasonic treatment for 15 min. $Na_2MoO_4{\cdot}2H_2O$ (0.73 mmol) was introduced in the above solution under vigorous stirring for 1 h. Then, 4.40 mmol thioacetamide (TAA) was added and diluted to 40 mL with pure water and ultrasonic operation for 30 min. Then, the homogeneous solution was transferred to a Teflon-lined stainless-steel autoclave and maintained at 200 °C for 24 h. The resultant black composite (SWCNHs-MoS_2) was dried at 80 °C after centrifugal washing with ethanol/water several times.

Synthesis of $ZnFe_2O_4$ and Fc-$ZnFe_2O_4$. $ZnFe_2O_4$ was prepared as mentioned in the SI. A series of products with different morphologies were prepared by adjusting the molar ratios of $Zn(Ac)_2$ and $FeCl_3{\cdot}6H_2O$ while other reaction parameters were unchanged (Table 1). $ZnFe_2O_4$ with different morphologies (50 mg) was dispersed in 10 mL of 0.5 wt % ethanol solution of Fc with ultrasonic treatment for 24 h. Then, the solution was added very slowly to 30 mL of 0.5 wt % poly(ethyleneimine) (PEI) solution and shaken overnight. The

Table 1. Summary of $Zn(Ac)_2$ and $FeCl_3{\cdot}6H_2O$ Molar Ratios, the Corresponding Morphologies of the Products, and the Photocurrent in This System

sample	$nZn(Ac)_2$ (mol)	$nFeCl_3{\cdot}6H_2O$ (mol)	morphology	average particle size (nm)	Ip (μA)
A		0.003	solid spherical	234.6	1.468
B	0.003	0.006	solid spherical	545.5	2.723
C	0.003	0.005	hollow spherical	156.4	6.588
D	0.003	0.003	nanogranular	132.5	5.023
E	0.005	0.003	solid spherical	496.2	3.610
F	0.006	0.003	hollow daisy	192.6	3.543
G	0.003		hollow spherical	1128.8	3.906

https://dx.doi.org/10.1021/acs.analchem.0c04485
Anal. Chem. 2021, 93, 2464−2470

composite (Fc-$ZnFe_2O_4$) separated by magnet was dispersed in 10 mL of water after washing with water and stored at 4 °C.

Preparation of the $ZnFe_2O_4$ and Fc-$ZnFe_2O_4$-Labeled Detection Antibody. $ZnFe_2O_4$ and Fc-$ZnFe_2O_4$ were activated by addition of 200 μL of 1-(3-dimethylaminopropyl)-3-ethylcarbodiimide hydrochloride (EDC) (20 mg·mL^{-1}) and 200 μL of *N*-hydroxysuccinimide (NHS) solution (10 mg·mL^{-1}), respectively. Subsequently, 2 mL of 0.1 mg·mL^{-1} prostate-specific antibody (detection antibody, Ab2) solution was added, shaken gently overnight at 4 °C to obtain $ZnFe_2O_4$ and Fc-$ZnFe_2O_4$-labeled Ab2, respectively (Ab2-Fc-$ZnFe_2O_4$ and Ab2-$ZnFe_2O_4$), resuspended in 2 mL of 0.1 M PBS (pH 7.4), and stored at 4 °C for further use.

Fabrication of the Dual-Heterojunction Immunoelectrode. Scheme 1A introduces the procedure of heterostructure immunoelectrode fabrication for PSA detection. Each cleaned glassy carbon electrode (GCE) was treated in 0.1 M Na_2SO_4 solution containing 1 wt % $HAuCl_4$ by potentiostatic electrodeposition for 10 s at −0.2 V to acquire a gold nanoparticle-modified electrode (Dp Au/GCE). A quantity of 10 μL of SWCNHs-MoS_2 was decorated on Dp Au/GCE by π−π stacking (SWCNHs-MoS_2/Dp Au/GCE),[32] rinsed with water and dried. Then, the modified electrode was immersed in 5 μL of 5 mM $AgNO_3$ and thioacetamide (TAA) solution for 30 min successively, so as to in situ generate Ag_2S (Ag_2S/SWCNHs-MoS_2/Dp Au/GCE). After rinsing with water, 5 μL of thioglycolic acid (TGA, 0.1 mM) was incubated for 1 h. Subsequently, the electrode activated by 20 μL of EDC and NHS for 2 h in succession was incubated with 6 μL of 10 μg·L^{-1} capture antibody (Ab1) at 4 °C overnight (Ab1/Ag_2S/SWCNHs-MoS_2/Dp Au/GCE). Finally, the nonspecific binding sites were sealed up by 3 μL of 1 wt % bovine serum protein (BSA) solution, and the uncombined biomolecules were removed by 0.1 M PBS (pH 7.4). The purposed immunoelectrode (BSA/Ab1/Ag_2S/SWCNHs-MoS_2/Dp Au/GCE) thus obtained was stored at 4°C for further use.

Immunoassay Development. Under the same external conditions, PSA with different concentrations (6 μL) was incubated with the proposed immunoelectrode at 37 °C for 30 min, then incubated with Ab2-Fc-$ZnFe_2O_4$ (6 μL) to complete the sandwich immunorecognition. After each operation, the electrodes were rinsed with 0.1 M PBS (pH 7.4) and the photocurrent signal was measured at 0 V under white light irradiation.

RESULTS AND DISCUSSION

Characteristics of Synthesized Materials. A series of products prepared with $Zn(Ac)_2$ and $FeCl_3·6H_2O$ are characterized by scanning electron microscopy (SEM), which exhibit in various forms of solid spherical, hollow spherical, nanogranular, and hollow daisy flower shapes (Figure S2A−G). When these composites are cured with Fc as the biological probe, respectively, the highest PEC signal is obtained from the regular and conformity hollow spherical one in the sandwich immune response to PSA (Table 1C). These hint that the hollow spherical nano-semiconductor synthesized by this method features a low density, high photoelectron conduction efficiency, large specific surface area, and unique nanocavity,[33] which can serve as a good carrier for curing Fc and is selected for the further experiments.

The hollow spherical structure of $ZnFe_2O_4$ with a shell thickness of about 48 nm and a homogeneous lattice characteristic can be observed by a transmission electron microscope (TEM) and high-resolution transmission electron microscope (HRTEM, Figure 1A and inset). The X-ray

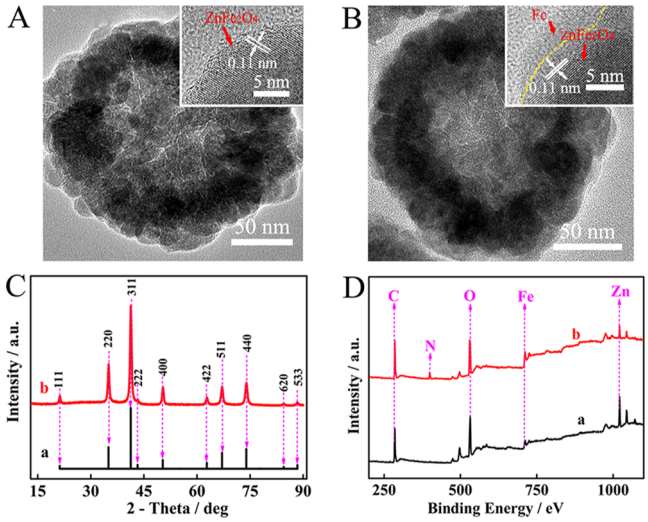

Figure 1. TEM images (inset: HRTEM) of (A) $ZnFe_2O_4$ and (B) Fc-$ZnFe_2O_4$. (C) (a) Powder diffraction file and (b) XRD pattern of $ZnFe_2O_4$. (D) XPS spectra of (a) $ZnFe_2O_4$ and (b) Fc-$ZnFe_2O_4$.

diffraction (XRD) pattern of as-synthesized $ZnFe_2O_4$ (Figure 1Cb) is in agreement with the standard spinel $ZnFe_2O_4$ structure (JCPDS, No. 22-1012, Figure 1Ca), demonstrating its face-centered cubic phase of the high purity and good crystal form.[34] Compared with $ZnFe_2O_4$, a layer of amorphous material exists on Fc-$ZnFe_2O_4$ with the shell thickness increasing to about 54 nm (Figure 1B and inset). In the overall survey of Fc-$ZnFe_2O_4$ X-ray photoelectron spectroscopic (XPS) spectra (Figure 1Db), C, N, O, Fe, and Zn elements appear. The nitrogen peak should be derived from PEI, and the Fe peak increases while the Zn peak decreases with the same mass of the composite. All of the above confirm that the curing sacrificial agent of the Fc-$ZnFe_2O_4$ nanocomposite has been synthesized.

The morphological changes and possible properties from the pristine SWCNHs to the Ag_2S/SWCNHs-MoS_2 sample are tracked by SEM and XPS. The Mott−Schottky (M−S) measurements are conducted at frequencies of 10 Hz to elucidate the different behaviors of nano-semiconductors (Figure S3). The negative slope of M−S plots for SWCNHs-MoS_2 is consistent with the behavior of a typical p-type semiconductor (Figure S3A), and the positive slopes for Ag_2S and Ag_2S/SWCNHs-MoS_2 materials are matched to the n-type (Figure S3B,C).[35] The S-shape M−S plots may indicate the formation of a Schottky junction between SWCNHs and MoS_2, and a peak appearing in Ag_2S/SWCNHs-MoS_2 suggests that the p−n heterojunction probably existed.[36,37] When MoS_2 is generated in situ of SWCNHs, the original thin flocs of the SWCNHs become denser and thicker (Figure 2A,B). The polycrystalline images with different d-spacing lattice distribution are observed in HRTEM (inset of Figure 2B), indicating the growth of MoS_2 on SWCNHs through the Schottky junction structure. With the formation of Ag_2S in situ on SWCNHs-MoS_2, the morphology changes from a thin floc to a mellow film. The XPS spectrum of the Ag_2S/SWCNHs-MoS_2 nanocomposite presents three elements of Mo, S, and Ag (Figure 2D(c)). In the S 2p fitting spectrum, the peaks at 160.8 and 161.9 eV are assigned to Ag_2S and MoS_2, respectively, the

https://dx.doi.org/10.1021/acs.analchem.0c04485
Anal. Chem. 2021, 93, 2464−2470

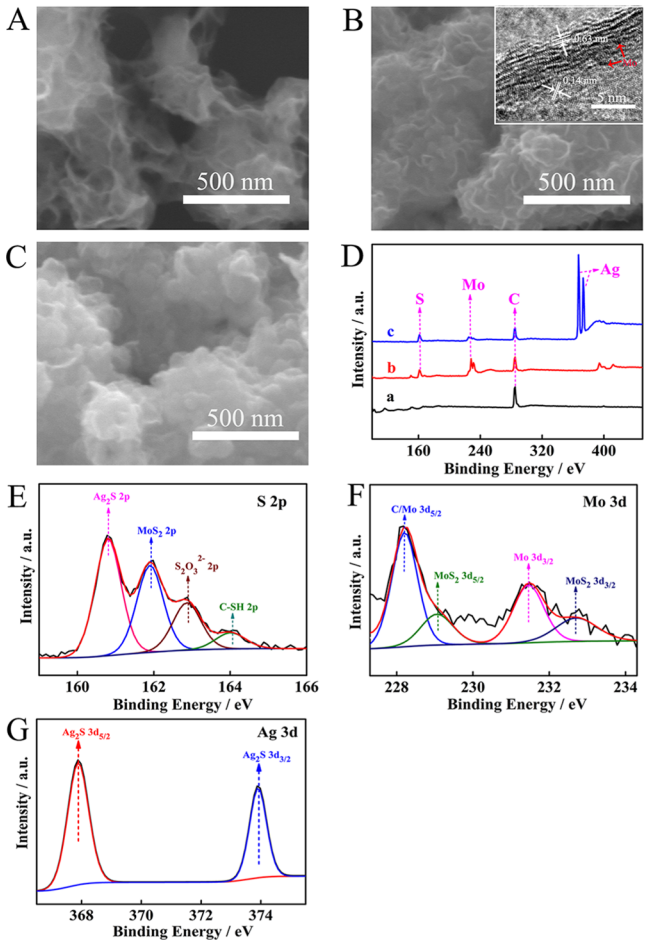

Figure 2. SEM images of (A) SWCNHs, (B) SWCNHs-MoS_2 (inset: HRTEM image), and (C) Ag_2S/SWCNHs-MoS_2. (D) XPS patterns of (a) SWCNHs, (b) SWCNHs-MoS_2, and (c) Ag_2S/SWCNHs-MoS_2. High-resolution XPS spectra of Ag_2S/SWCNHs-MoS_2 (E) S 2p, (F) Mo 3d, and (G) Ag 3d.

sub-peak located at 162.9 is probably the oxidation of thioacetamide to $S_2O_3^{2-}$, and the peak at 164.1 eV may be the reduction of sulfur in the residual TAA to the sulfhydryl group (Figure 2E).[38] Four peaks split that from the Mo 3d fitting spectrum are displayed in the binding energy region of Mo 3d (Figure 2F). The peaks situated at 228.2 and 231.5 eV are in the bonds of C−Mo and Mo−Mo, respectively, and the two shoulder peaks at 229.1 and 232.7 eV are related to Mo−S. These demonstrate the products in forms of molybdenum and molybdenum disulfide in situ on SWCNHs from the primary hexavalent molybdate (MoO_4^{2-}), and indicate the formation of the Schottky junction structure as well. The spin−orbit components of Ag $3d_{5/2}$ and $3d_{3/2}$ peaks are shifted to 368.0 and 373.9 eV (Figure 2G), respectively, implying the construction of the p−n heterojunction. Furthermore, when SWCNHs-MoS_2 and Ag_2S are successively modified on the Dp Au, the SEM, energy dispersive spectroscopy (EDS), and elemental mapping images demonstrating the elements of Au, Mo, C, Ag, and S are received and uniformly distributed (Figure S1). All of the above results suggest the successful preparation of Ag_2S/SWCNHs-MoS_2 nanocomposites with the dual-heterojunction structure.

Characterization of Stepwise Preparation of the Immunosensor. Electrochemical impedance spectroscopy (EIS) and PEC have been used to investigate the preparation process of BSA/Ab1/Ag_2S/SWCNHs-MoS_2/Dp Au/GCE. As displayed in Figure 3A, lower interfacial electron transfer

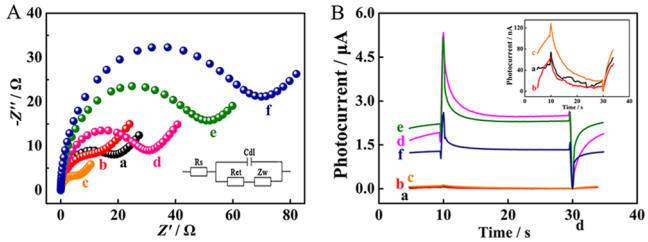

Figure 3. (A) Nyquist diagrams of EIS recorded from 0.01 Hz to 100 kHz in 4 mL of 0.1 M PBS (pH 7.4) containing 5 mM $[Fe(CN)_6]^{3-/4-}$. (B) PEC performances in 0.1 M PBS (pH 7.4): (a) bare GCE, (b) Dp Au/GCE, (c) SWCNHs-MoS_2/Dp Au/GCE, (d) Ag_2S/SWCNHs-MoS_2/Dp Au/GCE, (e) Ab1/Ag_2S/SWCNHs-MoS_2/Dp Au/GCE, and (f) BSA/Ab1/Ag_2S/SWCNHs-MoS_2/Dp Au/GCE.

resistances (Rets) are obtained after bare GCE is decorated with Dp Au and SWCNHs-MoS_2 in succession (curves b and c). The Rets increase successively with the consecutive modification of the Ag_2S, Ab1, and BSA (curves d−f). As shown in Figure 3B, the PEC signals level off when GCE is electrodeposited by gold nanoparticles (curves a and b), then gradually rise when the dual-heterojunction semiconductors are modified (curves c and d). While Ab1 and BSA are incubated in turn, the PEC signals are decreased continuously. These phenomena imply that the dual-heterojunction PSA immunoelectrodes have been synthesized (Scheme 1A).

Feasibility Investigation of the Dual-Heterojunction PEC Immunoassay. In the PEC immunoassay system, Ag_2S/SWCNHs-MoS_2 is coupled with Ab1 to act as a photocurrent generator to realize signal conversion on GCE electrodeposited with gold nanoparticles. The PSA reacts with Ab1 at 37 °C for 30 min and then incubates with Ab2-Fc-$ZnFe_2O_4$ under the same conditions. When the bio-nanoprobes are captured by the target, the dual-heterojunction PEC system will work under light. In this system, more Ab2-Fc-$ZnFe_2O_4$ can be captured by increasing the concentration of the target and a higher PEC signal can be induced.

In the heterostructure PEC system, it is found that a better photoelectric conversion efficiency can be obtained from white light than specific monochromatic light (Figure S6). White light with a power density of 12.6 mW·cm^{-2} as the irradiation source is selected in this work. To understand the role of a dual-heterojunction, control experiments to determine PSA have been carried out using immunoelectrodes modified with different materials. Figure S7 and Table S1 show that the superior PEC response is gained from the proposed dual-heterojunction PEC system (BSA/Ab1/Ag_2S/SWCNHs-MoS_2/Dp Au/GCE). Besides, Figure S7h shows that the higher PEC signal is acquired by the nanoprobes in the presence of Fc. It is concluded that this proposed immunosensor exhibits more excellent performance than other construction strategies.

Analytical Performance of the PEC Immune System. Figure 4C shows that the photocurrents of the dual-heterojunction PEC system increase with increasing PSA concentration. The derived calibration curve with a good linear correlation between the photocurrent intensity and the logarithm concentration of PSA is displayed in Figure 4D.

https://dx.doi.org/10.1021/acs.analchem.0c04485
Anal. Chem. 2021, 93, 2464−2470

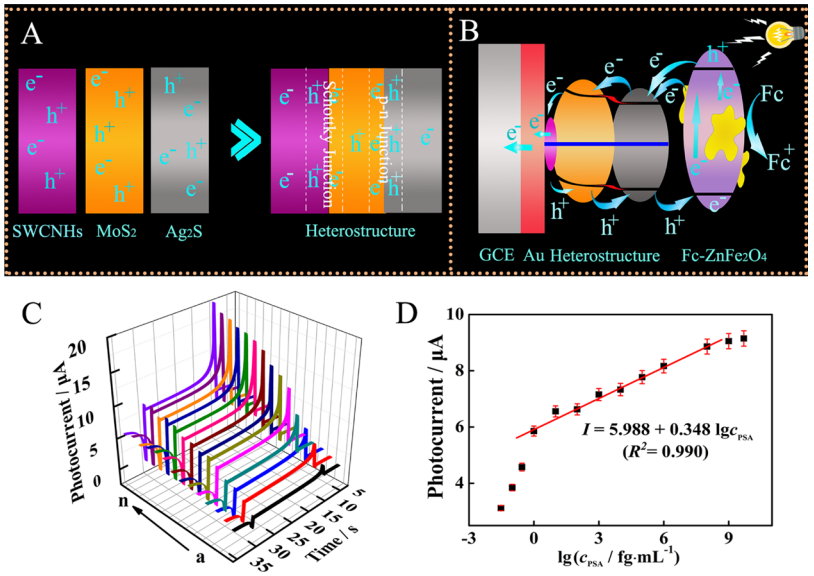

Figure 4. (A) Formation of the Ag_2S/MoS_2-SWCNH double junction composite. (B) While the Ab2-Fc-$ZnFe_2O_4$ captured, the possible mechanism of the PEC platform under white light. (C) Photocurrent−time responses of the proposed immunosensor to different concentrations of PSA (0, 3.0×10^{-8}, 1.0×10^{-7}, 3.0×10^{-7}, 1.0×10^{-6}, 1.0×10^{-5}, 1.0×10^{-4}, 1.0×10^{-3}, 1.0×10^{-2}, 1.0×10^{-1}, 1.0, 1.0×10^{2}, 1.0×10^{3}, and 5.0×10^{4} ng mL^{-1}). (D) Calibration curve of the photocurrent vs the logarithm concentration of PSA (error bars: standard deviation, $n = 3$).

The regression equation is $I = 5.988 + 0.348 \lg c_{PSA}$ from 1.0×10^{-6} to 1.0×10^{2} ng·mL^{-1} ($R^2 = 0.990$). The lowest detection limit is approximately 0.44 fg·mL^{-1} (S/N = 3), superior than the previously reported methods for PSA detection (Table S3). To explore the possible PEC mechanism of the signal amplification effect, the energy gaps (Eg's), the conduction band (CB), or valence band (VB) of SWCNHs-MoS_2, Ag_2S, and $ZnFe_2O_4$ are estimated in the SI, respectively. The mechanism can be explained as illustrated in Figure 4A,B possibly. When SWCNHs, MoS_2, and Ag_2S are combined into a dual-heterojunction structure, the Fermi level tends to be consistent, and the conduction band and valence band bend to form the built-in electric field. The CB of Ag_2S is below the CB of $ZnFe_2O_4$. While the Ab2-Fc-$ZnFe_2O_4$ is captured, the distance between the curing sacrificial agent and PEC platform is greatly reduced. Meanwhile, the photoinduced electrons from Fc can rapidly transfer to the CB of Ag_2S through the CB of $ZnFe_2O_4$, finally accepted by the electrode generating a stable anodic photocurrent. It further highlights the advantage of the curing sacrificial agent-induced dual-heterojunction PEC system.

Detection of PSA in Diluted Human Serum Samples. The applicability of this PSA sensing system has been assessed in real samples by the standard addition method (Table S2). When different concentrations of PSA are added into 50-fold diluted human serum (0.1 M PBS, pH 7.4), the spike recovery rate ranges from 98.0 to 102.0% with relative standard deviations (RSD) of 1.5−4.5%, demonstrating that this proposed PEC system can detect PSA in biological samples with acceptable performance.

Selectivity and Stability of the Proposed PEC System. As shown in Figure 5A, selectivity has been investigated by the carcinoembryonic antigen (CEA), α-fetoprotein (AFP), BSA, and the mixtures with PSA, testifying the sensor with improved selectivity. Figure 5B reveals that the intensity and shape of the current signal responses are stable corresponding to 1.0 fg·mL^{-1} PSA under repeated on−off irradiations over 600 s with a 1.8% relative standard deviation, suggesting the PEC immunosensor with good stability.

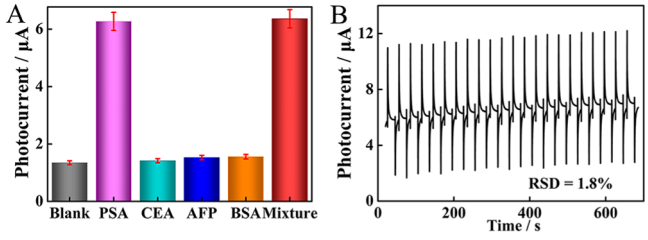

Figure 5. (A) Selectivity of the PEC immunosensor in blank, 100 fg·mL^{-1} PSA, 100 fg·mL^{-1} CEA, 100 fg·mL^{-1} AFP, 1 wt % BSA, and the mixture of 100 fg·mL^{-1} PSA, CEA, AFP, and 1 wt % BSA. (B) Stability of the PEC immunosensor towards 1.0 fg·mL^{-1} PSA.

CONCLUSIONS

In summary, this curing sacrificial agent-induced dual-heterojunction PEC immunosensing system with high sensitivity, good selectivity, and excellent stability has been developed for detection of PSA. Due to the built-in electric field, these semiconductor materials are more conducive to the effective separation of electrons and holes, which can widen the absorption range of light and improve the sensitivity. The strategy of the curing sacrificial agent can overcome the shortcomings of traditional PEC detection, reduce the detection background, shorten the distance between the sacrificial agent and semiconductor, amplify the photocurrent signal, and improve the stability of the PEC system. The novel PEC system is expected to stimulate more interest in the development of bioanalysis.

ASSOCIATED CONTENT

Supporting Information

The Supporting Information is available free of charge at https://pubs.acs.org/doi/10.1021/acs.analchem.0c04485.

https://dx.doi.org/10.1021/acs.analchem.0c04485
Anal. Chem. 2021, 93, 2464−2470

Reagents and apparatus; construction of the photoelectric platform; preparation of $ZnFe_2O_4$; SEM images of products prepared by $Zn(Ac)_2$ and $FeCl_3 \cdot 6H_2O$; Mott−Schottky (M−S) plots of semiconductors, the band gap, conduction band (CB), and valence band (VB); determination of SWCNHs-MoS_2, Ag_2S, and $ZnFe_2O_4$; optimization experiments of the irradiation light source; PEC signal of different sensor immune responses; detection of PSA in diluted human serum samples; and a comparison of various detection methods for PSA (PDF)

AUTHOR INFORMATION

Corresponding Author

Yingzi Fu − *Key Laboratory of Luminescence Analysis and Molecular Sensing, Ministry of Education, School of Chemistry and Chemical Engineering, Southwest University, Chongqing 400715, China;* orcid.org/0000-0003-4894-8549; Phone: +86-023-68252277; Email: fyzc@swu.edu.cn

Authors

Min Chen − *Key Laboratory of Luminescence Analysis and Molecular Sensing, Ministry of Education, School of Chemistry and Chemical Engineering, Southwest University, Chongqing 400715, China*

Fangjing Mo − *Key Laboratory of Luminescence Analysis and Molecular Sensing, Ministry of Education, School of Chemistry and Chemical Engineering, Southwest University, Chongqing 400715, China*

Hui Meng − *Key Laboratory of Luminescence Analysis and Molecular Sensing, Ministry of Education, School of Chemistry and Chemical Engineering, Southwest University, Chongqing 400715, China*

Cun Wang − *Key Laboratory of Luminescence Analysis and Molecular Sensing, Ministry of Education, School of Chemistry and Chemical Engineering, Southwest University, Chongqing 400715, China*

Jiang Guo − *Key Laboratory of Luminescence Analysis and Molecular Sensing, Ministry of Education, School of Chemistry and Chemical Engineering, Southwest University, Chongqing 400715, China*

Complete contact information is available at: https://pubs.acs.org/10.1021/acs.analchem.0c04485

Notes

The authors declare no competing financial interest.

ACKNOWLEDGMENTS

This work was supported by the National Natural Science Foundation of China (22077105, 21272188), the Natural Science Foundation Project of CQ CSTC (cstc2020jcyj-msxmX0854), and Innovation Foundation of Chongqing City for Postgraduate (CYB20089), China.

REFERENCES

(1) Shu, J.; Tang, D. *Anal. Chem.* **2020**, *92*, 363−377.
(2) Laskowski, F. A. L.; Nellist, M. R.; Qiu, J.; Boettcher, S. W. *J. Am. Chem. Soc.* **2019**, *141*, 1394−1405.
(3) Woods-Robinson, R.; Han, Y.; Zhang, H.; Ablekim, T.; Khan, I.; Persson, K. A.; Zakutayev, A. *Chem. Rev.* **2020**, *120*, 4007−4055.
(4) Medhi, R.; Marquez, M. D.; Lee, T. R. *ACS Appl. Nano Mater.* **2020**, *3*, 6156−6185.
(5) Wang, T.; Legut, D.; Fan, Y.; Qin, J.; Li, X.; Zhang, Q. *Nano Lett.* **2020**, *20*, 6199−6205.
(6) Shin, G. H.; Park, C.; Lee, K. J.; Jin, H. J.; Choi, S. Y. *Nano Lett.* **2020**, *20*, 5741−5748.
(7) Lu, K.; Liu, Y.; Lin, F.; Cordova, I. A.; Gao, S.; Li, B.; Peng, B.; Xu, H.; Kaelin, J.; Coliz, D.; Wang, C.; Shao, Y.; Cheng, Y. *J. Am. Chem. Soc.* **2020**, *142*, 12613−12619.
(8) Matanfack, G. A.; Taubert, M.; Guo, S.; Houhou, R.; Bocklitz, T.; Küsel, K.; Rösch, P.; Popp, J. *Anal. Chem.* **2020**, *92*, 11429−11437.
(9) Alam, A. U.; Deen, M. J. *Anal. Chem.* **2020**, *92*, 5532−5539.
(10) Ran, L.; Luo, B.; Gentle, I. R.; Lin, T.; Sun, Q.; Li, M.; Rana, M. M.; Wang, L.; Knibbe, R. *ACS Nano* **2020**, *14*, 8826−8837.
(11) Shao, Y.; Mei, S.; Lu, Y.; Zhang, M.; Sun, J.; Matyjaszewski, K.; Antonietti, M.; Yuan, J.; Wang, H. *Chem. Rev.* **2020**, *120*, 9363−9419.
(12) Lu, J.; Zheng, Z.; Yao, J.; Gao, W.; Zhao, Y.; Xiao, Y.; Li, J. *Small.* **2019**, *15*, No. 1904912.
(13) Liu, Y. X.; Wang, H. H.; Zhao, T. J.; Zhang, B.; Su, H.; Xue, Z. H.; Li, X. H.; Chen, J. S. *J. Am. Chem. Soc.* **2019**, *141*, 38−41.
(14) LaGasse, S. W.; Dhakras, P.; Watanabe, K.; Taniguchi, T.; Lee, J. U. *Adv. Mater.* **2019**, *31*, No. 1901392.
(15) Liu, S.; Zhang, X.; Gu, X.; Ming, D. *Biosens. Bioelectron.* **2019**, *143*, No. 111617.
(16) Unni, S. M.; Bhange, S. N.; Illathvalappil, R.; Mutneja, N.; Patil, K. R.; Kurungot, S. *Small* **2015**, *11*, 352−360.
(17) Sun, L.; Wang, R.; Ju, Q.; Xu, J. *Environ. Sci. Technol.* **2020**, *54*, 4409−4420.
(18) Zhang, P.; Lu, X. F.; Luan, D.; Lou, X. W. *Angew. Chem.* **2020**, *132*, 8205−8209.
(19) Han, F.; Song, Z.; Nawaz, M. H.; Dai, M.; Han, D.; Han, L.; Fan, Y.; Xu, J.; Han, D.; Niu, L. *Anal. Chem.* **2019**, *91*, 10657−10662.
(20) Hsu, J. C.; Cruz, E. D.; Lau, K. C.; Bouche, M.; Kim, J.; Maidment, A. D. A.; Cormode, D. P. *Chem. Mater.* **2019**, *31*, 7845−7854.
(21) Crisenza, G. E. M.; Mazzarella, D.; Melchiorre, P. *J. Am. Chem. Soc.* **2020**, *142*, 5461−5476.
(22) Wenderich, K.; Mul, G. *Chem. Rev.* **2016**, *116*, 14587−14619.
(23) Wang, G. L.; Yuan, F.; Gu, T.; Dong, Y.; Wang, Q.; Zhao, W. W. *Anal. Chem.* **2018**, *90*, 1492−1497.
(24) Wang, B.; Mei, L. P.; Ma, Y.; Xu, Y. T.; Ren, S. W.; Cao, J. T.; Liu, Y. M.; Zhao, W. W. *Anal. Chem.* **2018**, *90*, 12347−12351.
(25) Wang, B.; Xu, Y. T.; Lv, J. L.; Xue, T. Y.; Ren, S. W.; Cao, J. T.; Liu, Y. M.; Zhao, W. W. *Anal. Chem.* **2019**, *91*, 3768−3772.
(26) Chen, F. Z.; Han, D. M.; Chen, H. Y. *Anal. Chem.* **2020**, *92*, 8450−8458.
(27) Lin, Y.; Zhou, Q.; Tang, D. *Anal. Chem.* **2017**, *89*, 11803−11810.
(28) Chen, Min.; Wang, C.; Meng, H.; Mo, F.; Fu, Y. *Chem. Commun.* **2020**, *56*, 2300−2303.
(29) Ikeda, T.; Tahara, K.; Kadoya, T.; Tajima, H.; Toyoda, N.; Yasuno, S.; Ozawa, Y.; Abe, M. *Langmuir* **2020**, *36*, 5809−5819.
(30) Song, J.; Liu, H.; Lei, M.; Tan, H.; Chen, Z.; Antoshin, A.; Payne, G. F.; Qu, X.; Liu, C. *ACS Appl. Mater. Interfaces* **2020**, *12*, 8915−8928.
(31) Jiao, S.; Liu, L.; Wang, J.; Ma, K.; Lv, J. *Small* **2020**, *16*, No. 2001223.
(32) Björk, Jonas.; Hanke, Felix.; Palma, Carlos-Andres.; Samori, Paolo.; Cecchini, Marco.; Persson, Mats. *J. Phys. Chem. Lett.* **2010**, *1*, 3407−3412.
(33) Chen, A.; Zhao, M.; Zhuo, Y.; Chai, Y.; Yuan, R. *Anal. Chem.* **2017**, *89*, 9232−9238.
(34) Zhang, C.; Gu, Y.; Teng, G.; Wang, L.; Jin, X.; Qiang, Z.; Ma, W. *ACS Appl. Mater. Interfaces.* **2020**, *12*, 29883−29898.
(35) Jiang, Z. W.; Zou, Y. C.; Zhao, T. T.; Zhen, S. J.; Li, Y. F.; Huang, C. Z. *Angew. Chem.* **2020**, *132*, 3326−3332.
(36) Gelderman, K.; Lee, L.; Donne, S. W. *J. Chem. Educ.* **2007**, *84*, 685.

(37) Kirchartz, T.; Gong, W.; Hawks, S. A.; Agostinelli, T.; MacKenzie, R. C. I.; Yang, Y.; Nelson, J. *J. Phys. Chem. C* **2012**, *116*, 7672−7680.
(38) Mahanta, N.; Szantai-Kis, D. M.; Petersson, E. J.; Mitchell, D. A. *ACS Chem. Biol.* **2019**, *14*, 142−163.

https://dx.doi.org/10.1021/acs.analchem.0c04485
Anal. Chem. 2021, 93, 2464−2470